JACS
JOURNAL OF THE AMERICAN CHEMICAL SOCIETY
Article
pubs.acs.org/JACS

The Study of Multireactional Electrochemical Interfaces via a Tip Generation/Substrate Collection Mode of Scanning Electrochemical Microscopy: The Hydrogen Evolution Reaction for Mn in Acidic Solution

Kevin C. Leonard[†] and Allen J. Bard*

Center for Electrochemistry, Department of Chemistry and Biochemistry, University of Texas at Austin, Austin, Texas 78712, United States

Supporting Information

ABSTRACT: We report a new method of scanning electrochemical microscopy (SECM) that can be used to separate multireactional electrochemical interfaces, i.e., electrodes at which two or more reactions occur (and hence two partial currents flow) at the same time. This was done with a modified tip generation/substrate collection mode where the two reactions occur on the tip electrode, and the substrate electrode is held at a potential to collect only one of the products, allowing the determination of the individual partial currents. Thus, by using the substrate electrode current and the difference between the tip and substrate electrode currents, the two reactions occurring on the tip electrode can be separated. As a test case for this new method, we investigated proton reduction on Mn, a reaction that, because of the highly corrosive nature of Mn, to our knowledge has never before been directly measured. This test was carried out using a Mn tip electrode and a Pt substrate electrode. Using a three-dimensional COMSOL Multiphysics simulation, we were able to accurately determine the tip/substrate distance with this electrode, and by fitting simulations to experimental data, we were able to determine an exchange current density, $\log(j^0) = -4.7 \pm 0.7$ A cm^{-2}, for proton reduction on Mn in strong acid. This result corrects a literature value and was used in a pattern recognition algorithm reported in a companion manuscript.

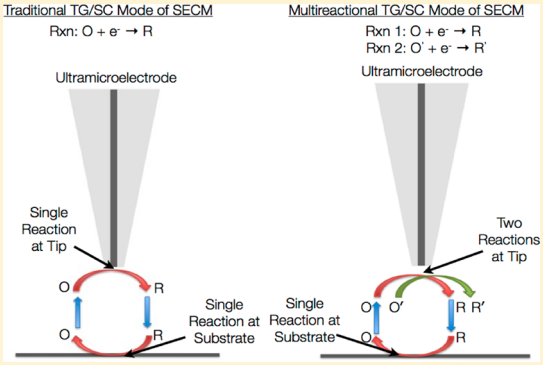

INTRODUCTION

Voltammetric measurements (i.e., current, I, vs potential, E) are frequently used to study reactions that occur at electrode surfaces. For example, with cyclic voltammetry (CV) one is able to control some variables of an electrochemical cell, such as potential or current, and measure how other variables fluctuate when the control variables are changed.[1] By perturbing the system in a controlled manner (e.g., changing sweep rate in CV), one is able to extract a wide range of information (e.g., electrochemical electron-transfer rate constants and the rate of decomposition of an unstable intermediate) from the measured current or potential.

However, in general with these techniques, the measured current at a given potential and time is the sum of all electrochemical reactions that are occurring. Thus, on multireactional electrochemical interfaces, i.e., an electrode where two or more electrochemical reactions occur at the same time or over the same potential range, one is unable to separate the individual partial currents and study the partial reactions. We suggest the notation for multireactional electrochemical interfaces as $\vec{E}_{1,p}$, $\vec{E}_{2,p}$, ..., where the subscript p indicates that the partial reactions, 1, 2, ..., are occurring in parallel, and the arrows indicate the direction of the reaction (a right arrow for a reduction and a left arrow for an oxidation). Table 1 illustrates possibilities for bireactional interfaces. These simultaneous reactions can be either competing reactions occurring over the same potential range or reactions that occur beyond the potential window of the solvent, where background reactions (e.g., the oxygen or hydrogen evolution reactions (OER and HER, respectively) for aqueous systems) dominate the measured current. The most important $\vec{E}_{1,p}\vec{E}_{2,p}$ systems are probably corrosion reactions, where metal oxidation occurs at the same potential as proton or oxygen reduction; it is this kind of reaction that is of interest in this paper.

Table 1. Representative Types of Bireactional Interfaces

reaction type	notation	example
two reductions	$\vec{E}_{1,p}\vec{E}_{2,p}$	O_2 and H^+ reduction
two oxidations	$\vec{E}_{1,p}\vec{E}_{2,p}$	H_2O and Cl^- oxidation
reduction and oxidation	$\vec{E}_{1,p}\vec{E}_{2,p}$	corrosion, e.g., H^+ reduction and Mn oxidation

Received: July 18, 2013
Published: September 24, 2013

dx.doi.org/10.1021/ja407395m | J. Am. Chem. Soc. 2013, 135, 15890−15896

While there are many techniques available to characterize and extract information from electrochemical systems, such as rotating ring-disk electrodes[2−4] and spectroelectrochemistry techniques,[5,6] one technique that has become very popular since its invention in 1989[7] is scanning electrochemical microscopy (SECM). SECM has been widely used in studying heterogeneous[8,9] and homogeneous[10,11] reaction kinetics, electrocatalysis,[12,13] semiconductor surfaces,[14,15] biological systems,[16,17] surface intermediates,[18,19] and electrochemical reactivity imaging,[20,21] among many other applications.[22,23] In general, SECM has some advantages over other techniques which include low *iR* drop, measurements at or near diffusional steady state, characterization capabilities on a wide variety of materials, and multiple modes of operation. For example, the substrate generation/tip collection mode of SECM has been used in studying H_2O_2 production during the oxygen reduction reaction on an alloy,[24] in which fabrication of a rotating ring-disk assembly would be difficult.

Here we report a new mode of SECM that utilizes a modified tip generation/substrate collection (TG/SC) mode[10] to investigate bireactional electrochemical interfaces. A schematic comparing the traditional TG/SC mode of SECM to the multireactional TG/SC mode of SECM is shown in Figure 1.

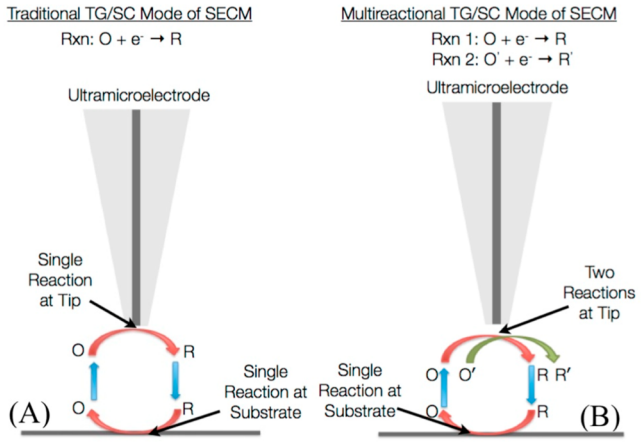

Figure 1. Schematic comparing (A) the traditional tip generation/substrate collection (TG/SC) mode of SECM to (B) the multireactional TG/SC mode of SECM. In the multireactional TG/SC mode, two reactions occur on the tip electrode while only one product is collected on the substrate electrode. This allows for separation of simultaneous reactions occurring on the tip electrode.

In traditional TG/SC (Figure 1A), a reactant O is reduced to R on an ultramicroelectrode (UME) tip, and a substrate electrode is held at a potential where R can be collected by oxidizing it back to O. Figure 1B shows the multireactional TG/SC mode for the $\vec{E}_{1,p}\vec{E}_{2,p}$ case, where two reduction reactions occur at the tip: O to R and O′ to R′. If the potential to oxidize R′ back to O′ is significantly different than the potential to oxidize R back to O, one can set the substrate potential to only oxidize R back to O and thus collect only R and not R′. If the tip/substrate distance is such that all R produced can be oxidized back to O (i.e., 100% collection efficiency), then the current attributed to each of the two reactions can be separated. Here, the tip current would be the combination of reaction 1 (O to R) and reaction 2 (O′ to R′), while the current on the substrate electrode would be the contribution from only reaction 1. Thus, the current produced from reaction 2 is the difference between the magnitudes of the tip current and the substrate current.

To demonstrate this multireactional TG/SC mode of SECM, we chose proton reduction on manganese as a study case. There were several reasons for this choice. First, Mn oxidizes to Mn^{2+} at very negative potentials (E^0 = −1.18 V vs NHE); thus, at any potential where proton reduction occurs (E^0 = 0 V vs NHE), Mn oxidation also takes place, making this system an $\vec{E}_{1,p}\vec{E}_{2,p}$ multireactional interface. Second, Mn^{2+} does not oxidize to Mn^{3+} until +1.5 V vs NHE, making proton reduction on Mn a good case for multireactional TG/SC because the potential to oxidize and collect H_2 is very different than the potential required to either reduce or oxidize Mn^{2+}. Finally, due to the ease of corrosion of Mn in acidic solutions, proton reduction on Mn has never, to our knowledge, been directly measured. In a companion paper, we report patterns that exist between the materials properties of the elements and their kinetics for the HER.[25] In our initial comparison, Mn was an outlier because the only published data for Mn were for water reduction rather than proton reduction.[26] Although we initially developed this method to measure proton reduction on Mn, it should have applications to many other systems in electrochemistry where simultaneous reactions occur.

EXPERIMENTAL SECTION

We employed a SECM system which used a fabricated Mn tip electrode and a Pt substrate electrode. For the Mn tip electrode, a piece of Mn (99.9%, Alfa Aesar, Ward Hill, MA) ∼2 cm × 2 cm was polished with sandpaper to remove the oxide layer and then sharpened, by hand, to a point using sand paper and a polishing wheel. After the Mn was sharpened to a point, a copper wire was soldered to the opposite end of the Mn. The Mn tip and the copper wire contact point were then completely coated with a two-part epoxy resin (Loctite Hysol, 1C&EPKC) and dried in air at 110 °C for 2 h. For drying, the Mn tip was held vertically in the drying oven using forceps. After cooling to room temperature, the Mn tip was exposed by gentle hand polishing with an ultrafine polishing paper (grit P2500).

After fabrication of the Mn electrode, its size and geometry were characterized by optical microscopy and vertical scanning interferometry.[27] Briefly, a Wyko NT9100 optical surface profiler (Veeco, New York) was used to examine the final tip dimensions and height difference from the epoxy insulating sheath.

The substrate electrode used for the SECM experiments was a 2 mm Pt disk electrode (CH Instruments, Austin, TX), which was polished with a 0.3 μm alumina suspension prior to use in the experiment. For all experiments, the electrolyte was an aqueous solution of 5 mM HBF_4 (Acros Organics, New Jersey) with 0.1 M $NaBF_4$ (Fluka, Switzerland) supporting electrolyte. A CH Instruments 920C SECM (Austin, TX) was used for all electrochemical experiments. To avoid any competing oxygen reduction reactions, the SECM stage was placed inside a sealed glovebag filled with UHP Ar gas, and the electrolyte was deaerated inside the glovebag for ∼2 min before starting the experiment. While the oxygen partial pressure was not measured directly, we verified negligible dissolved oxygen, because a negligible reduction current was observed on the Pt substrate electrode at potentials where Pt would reduce O_2. Cyclic voltammetry was performed on the Pt substrate electrode (50 cycles from −0.35 to 1.5 V vs Ag/AgCl at 100 mV s^{-1}) prior to any SECM experiments to activate it, giving it the ability to effectively oxidize H_2.

Approach curves to position the tip and substrate electrode in close proximity were performed by holding the tip potential at −1.4 V vs Ag/AgCl and the substrate at +0.1 V vs Ag/AgCl and approaching the tip to the substrate at 0.5 μm s^{-1}. Once the tip electrode was in position where 100% of the tip-generated H_2 was collected on the substrate electrode, a linear sweep voltammetry (LSV) experiment was performed by sweeping the Mn tip electrode from −1.5 V vs Ag/AgCl to 0 V vs Ag/AgCl at 1 mV s^{-1}.

dx.doi.org/10.1021/ja407395m | J. Am. Chem. Soc. 2013, 135, 15890−15896

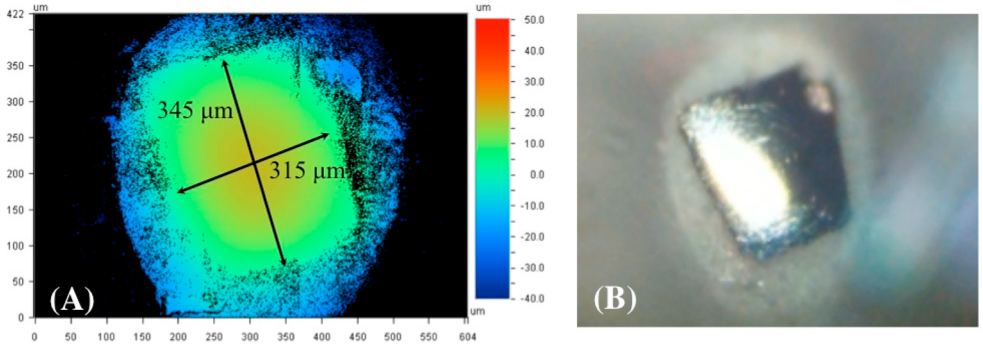

Figure 2. (A) Vertical scanning interferometry image and (B) optical microscopy image of custom Mn tip electrode. The electrode has a nearly rectangular shape with a 345 μm length and a 315 μm width.

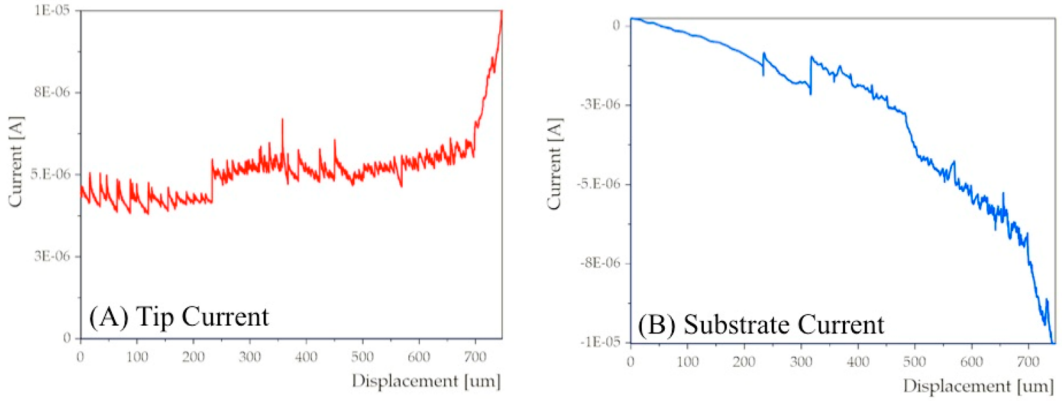

Figure 3. Approach curves of a Mn tip electrode and Pt substrate electrode showing (A) the tip current and (B) the substrate current as a function of the displacement of the tip electrode from the starting position. The approach curve was performed in a solution of 5 mM HBF_4 + 0.1 M $NaBF_4$ with the potential of the tip held at −1.4 V vs Ag/AgCl and the potential of the substrate held at +0.1 V vs Ag/AgCl.

Simulations were performed with COMSOL Multiphysics v. 4.3 on a Dell T7500 workstation. Details on parameters for the simulations are given in the Supporting Information.

RESULTS AND DISCUSSION

Scanning Electrochemical Microscopy Characterization. To measure proton reduction on Mn, we employed the multireactional SECM technique described in Figure 1. We chose the SECM setup with a Mn tip electrode and a Pt substrate electrode, because it had a high (near 100%) TG/SC efficiency and allowed accurate determination of the tip/substrate distance, which is essential for obtaining accurate kinetic information.[9,10] In our experiments, the approach curves were performed by holding the Mn tip electrode at a potential negative enough to stabilize it (i.e., prevent its corrosion), and the hydrogen produced on the Mn tip was collected by oxidation at the Pt substrate electrode. To study proton reduction on Mn, it would also have been possible to use a substrate generation/tip collection (SG/TC) mode of SECM, using a Mn substrate electrode with a more readily available Pt UME tip electrode. However, in this SG/TC mode (unless the substrate electrode diameter was about the same as the tip), the collection efficiencies are less than 100% and a known redox mediator is necessary to calibrate the system to obtain an accurate tip/substrate distance.[22] With the corrosiveness of Mn, it is not possible to use more conventional redox mediators, because at all potentials Mn either is oxidized to Mn^{2+} or is at a potential where hydrogen is being produced. Thus, we felt that the best method for obtaining an accurate tip/substrate distance was to use a Mn tip electrode and a Pt disk substrate electrode. While this choice involved fabrication of the Mn tip, it removed much of the ambiguity that would be involved with the SG/TC mode.

The Mn tip electrode was fabricated as described in the Experimental Section. Vertical scanning interferometry (VSI) and optical microscopy were used to characterize the electrode shape and size (Figure 2).[27] Here, the Mn tip electrode had a nearly rectangular shape with a length of 345 μm and a width of 315 μm. Also, as shown in the VSI image, the Mn electrode protrudes ∼10 μm from the epoxy insulation. While this tip electrode is large compared to most SECM tips, it could be approached sufficiently close to the Pt substrate to carry out the desired measurements, and its unique geometry could be simulated to account for its shape.

The first step in obtaining the heterogeneous electron transfer reaction rate constant for proton reduction on Mn was to record an approach curve and obtain a close tip/substrate distance. Figure 3 shows the tip current and substrate current as a function of displacement of the tip electrode from its starting position (i.e., the approach curve). The approach curve was performed in an aqueous solution of 5 mM HBF_4 with 0.1 M $NaBF_4$ supporting electrolyte. The potential of the tip held at −1.4 V vs Ag/AgCl and the potential of the substrate held at +0.1 V vs Ag/AgCl. The approach curve shows positive feedback for H_2 production at the tip and H_2 oxidation at the Pt substrate, and at very close distances, the tip current and substrate current are equal, indicating ∼100% collection efficiency. Many oscillations of increasing and decreasing

dx.doi.org/10.1021/ja407395m | J. Am. Chem. Soc. 2013, 135, 15890−15896

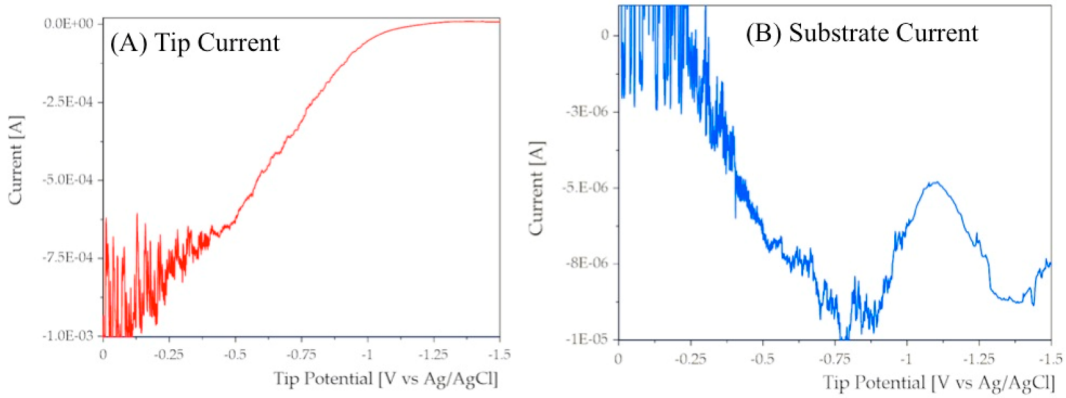

Figure 4. (A) Tip current and (B) substrate current as a function of tip potential for a LSV experiment using a Mn tip electrode and Pt substrate electrode in 5 mM HBF_4 + 0.1 M $NaBF_4$. The substrate potential was held at +0.1 V vs Ag/AgCl while the tip potential was scanned from −1.5 V vs Ag/AgCl to 0 V vs Ag/AgCl at a scan rate of 1 mV s^{-1}.

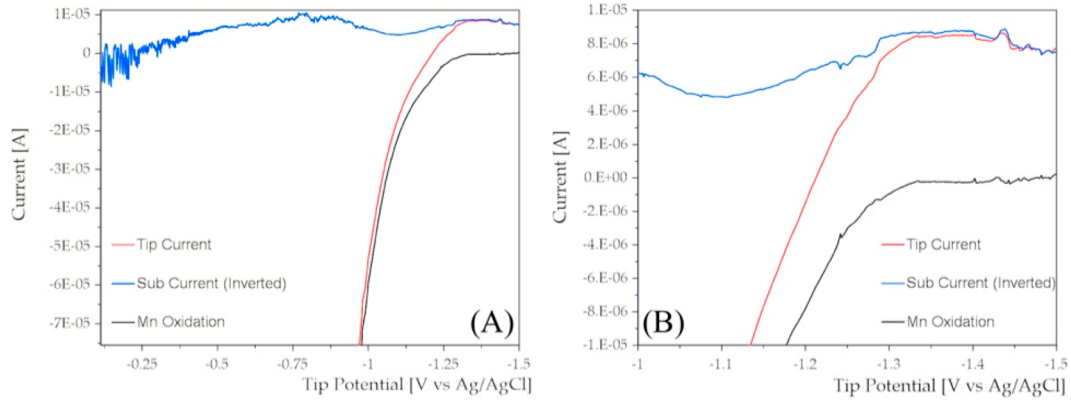

Figure 5. The total tip current along with the portions that are related to proton reduction and Mn oxidation at two different scales as a function of tip potential for a LSV experiment using a Mn tip electrode and Pt substrate electrode in 5 mM HBF_4 + 0.1 M $NaBF_4$. The substrate potential was held at +0.1 V vs Ag/AgCl, while the tip potential was scanned from −1.5 V vs Ag/AgCl to 0 V vs Ag/AgCl at a scan rate of 1 mV s^{-1}. The inverted substrate current is the portion of the current that results from the proton reduction reaction, and subtraction of the tip current from the inverted substrate current gives the portion that results from the Mn oxidation reaction.

currents on both the tip and substrate were observed due to hydrogen bubble formation and release occurring on the tip electrode. However, even with this bubble formation, we were still able to get an approach curve where the tip/substrate distance can be accurately obtained.

After the approach curve was complete and the tip was positioned close to the substrate, LSV was performed on the tip electrode while collecting the produced hydrogen on the Pt substrate. Figure 4 shows the tip current and substrate current as a function of tip potential for the LSV experiment. The solution was the same as used for the approach curve (5 mM HBF_4 + 0.1 M $NaBF_4$), and the substrate potential was held at +0.1 V vs Ag/AgCl while the tip potential was scanned from −1.5 V vs Ag/AgCl to 0 V vs Ag/AgCl at a scan rate of 1 mV s^{-1}. Note that the tip CV shows no potential range with zero current, since hydrogen production and/or Mn oxidation occurs at all potentials. At the beginning of the LSV, the tip is at a potential where the Mn is stable and the only reaction occurring on the tip is the HER. We were able to measure directly the tip-produced hydrogen from the substrate current due to the close distance and 100% collection efficiency. Once the tip potential reaches ∼−1.3 V vs Ag/AgCl, Mn oxidation begins. However, the substrate is still collecting and measuring the produced H_2. It is not until much less negative tip potentials (∼−0.25 V vs Ag/AgCl) where hydrogen is no longer collected on the substrate and the tip current is dominated by Mn oxidation. As with the approach curves, bubble formation on both the tip and substrate electrode can produce variations ("bubble noise") and larger events. In Figure 4B, there is a large bubble event that occurs on the substrate electrode for times corresponding to a tip potential from −1.25 to −0.8 V vs Ag/AgCl. However, this is in the regime where the HER is mass transfer controlled, and thus it will not have an effect on determination of the kinetics for proton reduction on Mn. In fact, in this region, the tip is covered with bubbles, but dissolved hydrogen continues to diffuse to the substrate.

As stated above, the substrate current is the portion of the tip current that results from proton reduction on Mn, while subtraction of the substrate current from the tip current yields the portion of the current that is due to Mn oxidation. Figure 5 shows the total tip current along with the portions that are related to proton reduction (inverted substrate current) and Mn oxidation as a function of tip potential. Examination of Figure 5 shows that, at potentials from −1.5 to −1.3 V vs Ag/AgCl, there is very good agreement between the tip current (total HER) and inverted substrate current (hydrogen oxidation reaction, HOR). Even small features due to bubble formation on the tip are observable on the substrate. Then, as

dx.doi.org/10.1021/ja407395m | J. Am. Chem. Soc. 2013, 135, 15890−15896

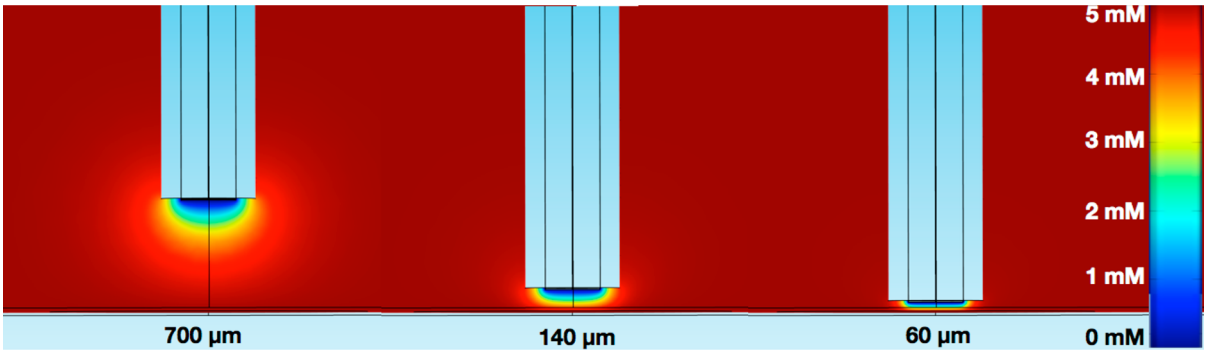

Figure 6. COMSOL Multiphysics simulations showing H^+ concentration at three different tip/substrate distances (700, 140, and 60 μm) for the 3D approach curve simulations.

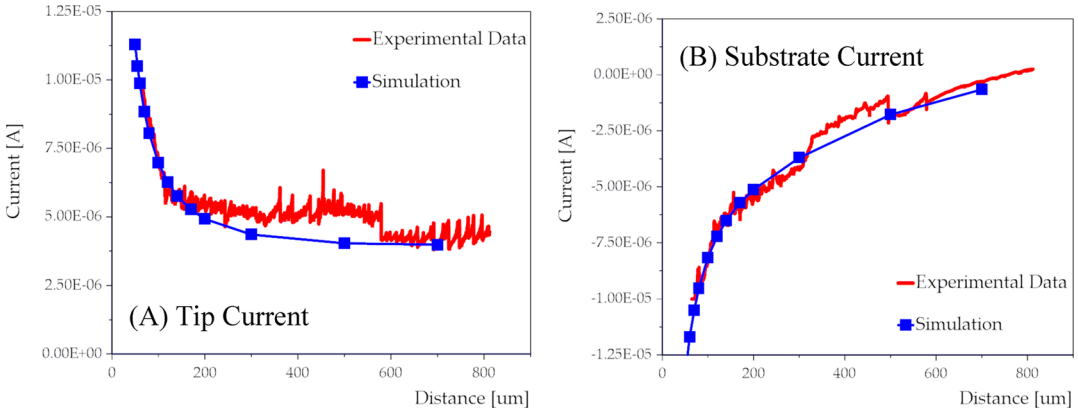

Figure 7. Three-dimensional COMSOL Multiphysics simulations of (A) the tip current and (B) the substrate current along with the experimental data for the approach curve using the Mn tip electrode and Pt substrate electrode. Using the simulation, it was determined that the final tip/substrate distance was 65 μm. Simulation parameters were $C_{init,H}{}^+ = 5$ mM, $D_{H}{}^+ = 7.9 \times 10^{-5}$ cm^2 s^{-1}, and $D_{H_2} = 4.5 \times 10^{-5}$ cm^2 s^{-1}.

the potential becomes less negative, the Mn oxidation reaction begins to dominate the tip current, but as stated above, we are still able to measure proton reduction on Mn from the collection of H_2 on the substrate.

Three-Dimensional Multiphysics Simulations. 3D COMSOL Multiphysics simulations of the approach curve were performed to obtain the tip/substrate distance. Details on all parameters used for the simulations are given in the Supporting Information. Because the fabricated Mn tip electrode had a rectangular shape and protruded ~10 μm from the insulating sheath, we simulated the approach curves using a 3D geometry, which mimicked the size, shape, and protrusion of the tip and substrate electrode, as opposed to the more conventional 2D axial-symmetric geometry appropriate for disk electrodes. In the Supporting Information, Figure S1 shows the cell geometry and tip geometry used for simulating the SECM experiment.

During the approach curve, the potentials of the tip and substrate electrode are such that both hydrogen evolution on the tip and hydrogen oxidation on the substrate are mass transfer controlled. Thus, to obtain the concentrations of both H_2 and H^+ everywhere throughout the 3D geometry, Fick's second law of diffusion (Supporting Information, eq S1) was solved using mass transfer controlled concentration boundary conditions on both the tip and substrate electrode and the literature reported values of 7.9×10^{-5} cm^2 s^{-1} for the diffusion coefficient of H^+ [28] and 4.5×10^{-5} cm^2 s^{-1} for the diffusion coefficient of H_2.[29] The currents on the tip and substrate electrode were calculated using Fick's first law of diffusion (Supporting Information, eq S2).

Using the parametric sweep function of COMSOL 4.3, we were able to automatically calculate the concentration profiles and the tip and substrate current for 13 different tip/substrate distances. Figure 6 shows the H^+ concentration profile for three different tip/substrate distances. Figure 7 shows that the simulated tip and substrate currents agree very well with the experimentally measured current after adjusting the $z = 0$ point for the best fit, and this yields the final tip/substrate distance as 65 μm.

Once the tip/substrate distance was known, we simulated the potential sweep on the tip to obtain the heterogeneous electron-transfer rate constant, k°_{eff}, for proton reduction on Mn. For the potential sweep experiment, Butler–Volmer kinetics were assumed for the flux boundary condition on the tip electrode. Figure 8 shows the experimental data for the portion of the current that is attributed to proton reduction on Mn, with a best-fit simulation. By fitting the simulation results to the experimental data, we obtain a kinetic rate constant for 5 mM acid of $k^\circ_{eff} = 3.7 \times 10^{-4}$ cm s^{-1} and $\alpha = 0.4$.

The goal of this experiment was to compare the exchange current density for proton reduction on Mn to a previously reported value in strong acid that deviated significantly in a pattern recognition study (companion manuscript).[25] The maximum concentration of acid we could use in our SECM experiment was 5 mM, because at higher concentrations bubble formation greatly distorted the data and kinetic information was not obtainable. However, to compare our rate constant data

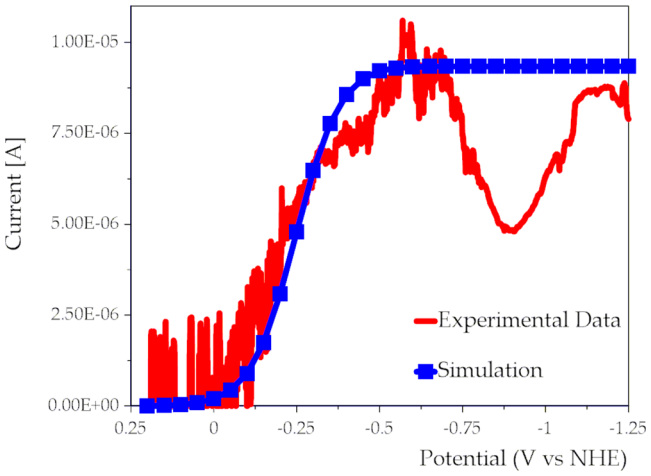

Figure 8. Experimental data for the portion of the current that is attributed to proton reduction on Mn, with a best-fit simulation calculated using COMSOL Multiphysics. By fitting the simulation results to the experimental data, we obtain kinetic rate constant parameters of $k^0_{eff} = 3.7 \times 10^{-4}$ cm s^{-1} and $\alpha = 0.4$.

with the values for the other elements (which were taken in concentrations of acid ranging from 0.1 to 1 M), we simulated proton reduction in strong acid using the rate constants obtained in 5 mM acid to estimate the exchange current density in either 0.1 or 1 M acid. This was accomplished by carrying out a 1D COMSOL Multiphysics simulation, and simulating a potential sweep using Butler–Volmer kinetics for the flux boundary conditions. From the simulation results, Tafel lines were drawn to obtain the exchange current densities (Figure 9). Tafel lines can be somewhat ambiguous, so in an effort to find the boundary limits on the exchange current density, we determined values of $\log(j^0)$ in 1 and 0.1 M acid to be −4.0 and −5.3 A cm^{-2}, respectively. The average of these two results yields $\log(j^0) = -4.7 \pm 0.7$ A cm^{-2} for use in the pattern recognition study.

Measurement of Proton Reduction on Fe. To verify the results we obtained for proton reduction on Mn, we also used the TG/SC mode of SECM to investigate proton reduction on Fe, another corrosive metal. Fe oxidation starts at −0.44 V vs NHE, but because of the sluggish HER kinetics, significant proton reduction does not occur until more negative potentials. Thus, there is a region on Fe where neither Fe oxidation nor H^+ reduction occurs, so it is easier to measure the kinetics of the HER on Fe than on Mn by conventional methods. It is a good test case to demonstrate this use of the TG/SC SECM technique. As described in the Supporting Information, we used the same method to obtain an exchange current density for Fe in strong acid with an Fe tip. Using this method, we obtained $\log(j^0) = -6.0 \pm 0.8$ A cm^{-2}. The known exchange current density for proton reduction on Fe is $\log(j^0) = -5.8$ A cm^{-2}, which is in very good agreement with the measurement we obtained using the TG/SC SECM technique.

CONCLUSIONS

We report a new method of TG/SC SECM that can be used to separate partial currents at multireactional electrochemical interfaces. If two separate partial reactions occur on the tip electrode and one can hold the substrate electrode to collect only the products of one of them, the two tip reaction currents can be separated. As a test case for this method, we investigated proton reduction on easily corroded Mn and estimated the previously unmeasured exchange current density for the HER. This test was carried out using a Mn tip electrode and Pt substrate electrode held at a potential where hydrogen is oxidized. By comparing a three-dimensional Multiphysics simulation to an experimental approach curve, we could accurately determine the tip/substrate distance. By fitting a simulated current–potential curve to an experimental one, we

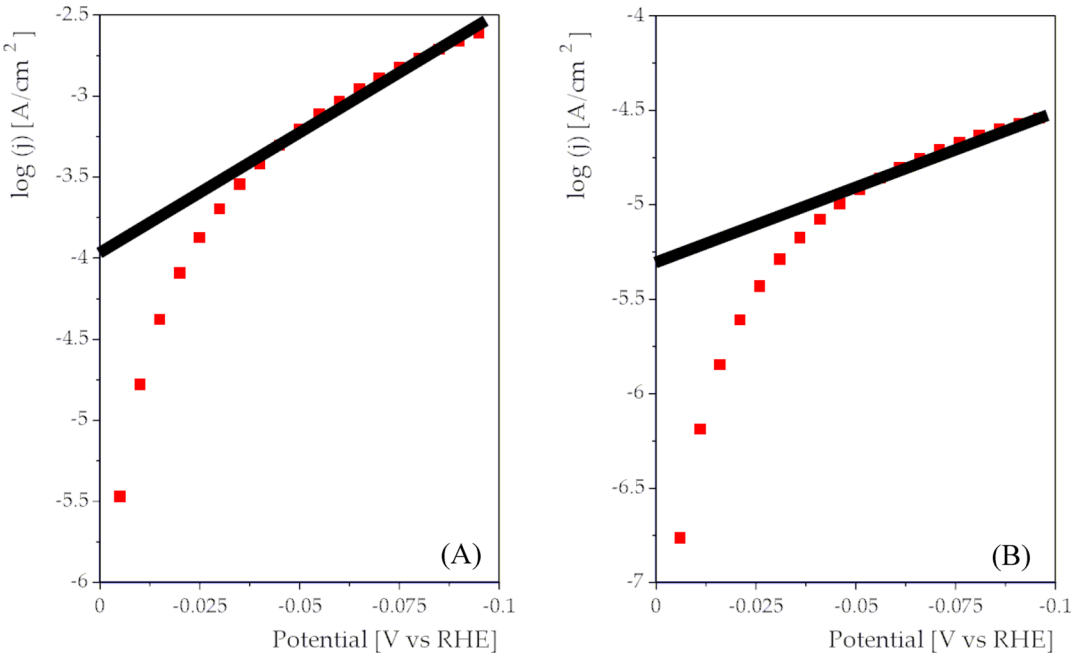

Figure 9. Simulations of Tafel curves using the kinetic rate constants obtained for Mn in acid concentrations of (A) 1 and (B) 0.1 M to determine $\log(j^0)$ for proton reduction on Mn in strong acid. We determined the average value of $\log(j^0)$ for proton reduction on Mn in strong acid to be −4.7 ± 0.7 A cm^{-2}.

dx.doi.org/10.1021/ja407395m | J. Am. Chem. Soc. 2013, 135, 15890–15896

measured an exchange current density, $\log(j^0)$, of -4.7 ± 0.7 A cm^{-2} for proton reduction on Mn in strong acid; this agreed well with that predicted by a pattern recognition algorithm reported in a companion manuscript.[25]

■ ASSOCIATED CONTENT

Supporting Information

COMSOL simulation and other experimental details. This material is available free of charge via the Internet at http://pubs.acs.org

■ AUTHOR INFORMATION

Corresponding Author

ajbard@mail.utexas.edu

Present Address

[†]K.C.L.: Center for Environmentally Beneficial Catalysis, Department of Chemical & Petroleum Engineering, The University of Kansas, Lawrence KS 66045

Notes

The authors declare no competing financial interest.

■ ACKNOWLEDGMENTS

This work was funded by a Fondazione Oronzio e Niccolò De Nora Fellowship in Applied Electrochemistry (KCL), the National Science Foundation (CHE-1111518), and the Robert A. Welch Foundation (F-0021).

■ REFERENCES

(1) Bard, A. J.; Faulkner, L. R. *Electrochemical Methods: Fundamentals and Applications*; 2nd ed.; John Wiley & Sons, Inc.: New York, 2001.
(2) Paulus, U. A.; Schmidt, T. J.; Gasteiger, H. A.; Behm, R. J. *J. Electroanal. Chem.* **2001**, *495*, 134−145.
(3) Markovic, N. M.; Gasteiger, H. A.; Ross, P. N. *J. Phys. Chem.* **1995**, *99*, 3411−3415.
(4) Kamin, R.; Wilson, G. *Anal. Chem.* **1980**, *52*, 1198−1205.
(5) Abruña, H. D., Ed. *Electrochemical Interfaces: Modern Techniques for In-Situ Interface Characterization*; VCH: New York, 1991.
(6) Jeanmaire, D. L.; Van Duyne, R. P. *J. Electroanal. Chem. Interfacial Electrochem.* **1977**, *84*, 1−20.
(7) Bard, A. J.; Fan, F.-R. F.; Kwak, J.; Lev, O. *Anal. Chem.* **1989**, *61*, 132−138.
(8) Sun, P.; Mirkin, M. V. *Anal. Chem.* **2006**, *78*, 6526−6534.
(9) Zhou, J.; Zu, Y.; Bard, A. J. *J. Electroanal. Chem.* **2000**, *491*, 22−29.
(10) Zhou, F.; Unwin, P. R.; Bard, A. J. *J. Phys. Chem.* **1992**, *4924*, 4917−4924.
(11) Treichel, D. A.; Mirkin, M. V.; Bard, A. J. *J. Phys. Chem.* **1994**, *98*, 5751−5757.
(12) Minguzzi, A.; Alpuche-Aviles, M. A.; Rodríguez López, J.; Rondinini, S.; Bard, A. J. *Anal. Chem.* **2008**, *80*, 4055−4064.
(13) Fernández, J. L.; Walsh, D. A.; Bard, A. J. *J. Am. Chem. Soc.* **2004**, *127*, 357−365.
(14) Lee, J.; Ye, H.; Pan, S.; Bard, A. J. *Anal. Chem.* **2008**, *80*, 7445−7450.
(15) Park, H. S.; Kweon, K.; Ye, H.; Paek, E.; Bard, A. J. *J. Phys. Chem. C* **2011**, *115*, 17870−17879.
(16) Zhao, C.; Wittstock, G. *Biosens. Bioelectron.* **2005**, *20*, 1277−1284.
(17) Kaya, T.; Nagamine, K.; Oyamatsu, D.; Shiku, H.; Nishizawa, M.; Matsue, T. *Lab Chip* **2003**, *3*, 313−317.
(18) Rodríguez-López, J.; Alpuche-Avilés, M. A.; Bard, A. J. *J. Am. Chem. Soc.* **2008**, *130*, 16985−18995.
(19) Park, H. S.; Leonard, K. C.; Bard, A. J. *J. Phys. Chem. C* **2013**, *117*, 12093−12102.
(20) Wilson, N. R.; Guille, M.; Dumitrescu, I.; Fernandez, V. R.; Rudd, N. C.; Williams, C. G.; Unwin, P. R.; Macpherson, J. V. *Anal. Chem.* **2006**, *78*, 7006−7015.
(21) Patel, A. N.; Collignon, M. G.; O'Connell, M. A.; Hung, W. O. Y.; McKelvey, K.; Macpherson, J. V.; Unwin, P. R. *J. Am. Chem. Soc.* **2012**, *134*, 20117−20130.
(22) Bard, A. J.; Mirkin, M. V. *Scanning Electrochemical Microscopy*, 2nd ed.; CRC Press: Boca Raton, FL, 2012.
(23) Amemiya, S.; Bard, A. J.; Fan, F.-R. F.; Mirkin, M. V.; Unwin, P. R. *Annu. Rev. Anal. Chem.* **2008**, *1*, 95−131.
(24) Shen, Y.; Träuble, M.; Wittstock, G. *Anal. Chem.* **2008**, *80*, 750−759.
(25) Leonard, K. C.; Bard, A. J. *J. Am. Chem. Soc.* **2013**, DOI: 10.1021/ja407394q, (preceding paper in this issue).
(26) Belanger, A.; Vijh, A. *J. Electrochem. Soc.* **1974**, *121*, 225−230.
(27) Chang, J.; Leonard, K. C.; Cho, S. K.; Bard, A. J. *Anal. Chem.* **2012**, *84*, 5159−5163.
(28) Macpherson, J. V.; Unwin, P. R. *Anal. Chem.* **1997**, *69*, 2063−2069.
(29) Ferrell, R. T.; Himmelblau, D. M. *AIChE J.* **1967**, *13*, 702−708.